Computation of dynamic loads exerted by regular water waves on a vertical cylinder with application to offshore wind turbine

Gustavo Ríos Rodríguez[1], Laura Battaglia[1,2], Sissy Morawietz[3], Marco Schauer[3]

[1]*Centro de Investigación de Métodos Computacionales (CIMEC) - UNL/CONICET*
Predio CONICET Santa Fe, Colectora Ruta Nac. 168, Km 472, Paraje El Pozo, 3000, Santa Fe, Argentina
gusadrr@santafe-conicet.gov.ar, lbattaglia@santafe-conicet.gov.ar
[2]*Grupo de Investigación en Métodos Numéricos en Ingeniería (GIMNI) - UTN FRSF*
Lavaisse 610, 3000, Santa Fe, Argentina
[3]*Institut für Statik, Technische Universität Braunschweig*
Beethovenstraße 51, 38106 Braunschweig, Germany
s.morawietz@tu-braunschweig.de, m.schauer@tu-braunschweig.de

Abstract. Wave forces on near-shore structures constitute relevant information to the design and verification of structural pieces. This wave loads are particularly important to design reliable piles and foundation of marine platforms or wind turbines. To investigate the dynamic effects of such forces a numerical wave tank is set in a finite volume Navier-Stokes solver. In the wave tank a vertical cylinder which represents the wind turbines tower is affected by free surface waves. Specific inlet and outlet boundary conditions available as part of OpenFoam distributions are included. Inlet boundary conditions are allowed to recreate either regular and focused wave conditions, while outlet conditions are established in order to avoid non physical reflections of surface waves on the artificial limits of the domain. The results obtained for regular waves are compared with experimental measurements, numerical studies and the Morison equation reference. The wave loads are also used to simulate an offshore wind turbine where wind loads and soil-structure interaction are considered. Further studies are performed with focused wave groups and breaking waves.

Keywords: wave forces, fluid structure interaction, numerical wave tank, volume of fluid, soil-structure-interaction.

1 Introduction

Water wave forces on semi-submerged structures have been typically quantified by experimental studies, semi-empirical rules [1] or, more recently, numerical simulations [2]. In the last case, numerical wave tanks (NWT) have been developed, where the inlet wave generation strategy and the outlet boundary conditions require proper settings to reproduce the physical wave effects [2, 3].

Here, the dynamic analysis of a near-shore wind turbine pile is performed, where wind and wave forces are considered, taking into account the soil-structure interaction. As a novelty, the wave dynamical forces are included from a computational fluid dynamic (CFD) study, and applied by a specific projection method previously developed [4] over the submerged part of the structure. The preliminary results shown here were obtained for a test case consisting in a semisubmerged cylinder of reduced dimensions submitted to surge, and properly scaled later to the pile geometry.

2 Numerical Approach

In this work, the approach used to analyze with numerical methods the dynamic response of a 5 MW rated power offshore wind turbine (OWT) is performed in the following manner. First, the action of water waves on a small rigid vertical cylinder in a numerical wave tank is simulated with the interFoam solver from the OpenFoam library. The main objective of this step is to compute pressure distributions and therefore horizontal forces which

are well validated by other numerical simulations as well as experimental results. Second order waves of the Stokes II family are considered. Then, the fluid dynamic loads on the small vertical cylinder are scaled in order to take into account the real size of the OWT pile. To this end, the relative depth as well as all the characteristic parameters that define the kind of wave (Stokes II) are kept the same. Afterwards, the maximum horizontal wave force is estimated with the Morison equation together with experimental correlations to compute approximated values for the drag and inertia coefficients for unsteady oscillatory flows around cylinders. The maximum horizontal force calculated as result of this scaling process is compared to values presented in the work of [5]. Then, the pressure on the small vertical cylinder is scaled in order to meet this value. Next, the loads due to the scaled pressure distribution are transferred from the fluid flow mesh on the cylinder surface to the structure mesh. Since the nodes of fluid and structure meshes do not coincided. A projection algorithm is used. Afterwards, the pressure on the structure mesh is translated to nodal forces which are used as input to the coupled FEM-SBFEM solver. In the coming sections, each of these stages are explained in more detail.

2.1 Coupled FEM-SBFEM approach

Here the coupled FEM-SBFEM approach is described very briefly, more details about the mathematical formulation and the efficient, massively parallel implementation can be found in [6]. The displacement-based equation of motion can be written as

$$\mathbf{M}\frac{d^2\mathbf{u}}{dt^2} + \mathbf{C}\frac{d\mathbf{u}}{dt} + \mathbf{K}\mathbf{u} = \mathbf{p} \tag{1}$$

at an arbitrary time step, where the matrices $\mathbf{M}$, $\mathbf{C}$ and $\mathbf{K}$ denotes mass, damping and stiffness, respectively. The vector $\mathbf{u}$ and its derivatives in time $\frac{d\mathbf{u}}{dt} = \dot{\mathbf{u}}$ and $\frac{d^2\mathbf{u}}{dt^2} = \ddot{\mathbf{u}}$ represent the nodal displacement, velocity and acceleration. The vector $\mathbf{p}$ represents the applied nodal forces. The implicit Newmark time integration scheme is considers to solve the time period T subdivided into n times steps [7]. This yields:

$$\mathbf{M}\ddot{\mathbf{u}}_{t_{n+1}} + \mathbf{C}\dot{\mathbf{u}}_{t_{n+1}} + \mathbf{K}\mathbf{u}_{t_{n+1}} = \mathbf{p}_{t_{n+1}}\,. \tag{2}$$

To couple the near-field (FEM) with the far-field (SBFEM), the entries of the matrices in Eq. (1) have to be split into the near-field and far-field, which results in the FEM equation:

$$\begin{bmatrix} \mathbf{M}_{\Omega\Omega} & \mathbf{M}_{\Omega\Gamma} \\ \mathbf{M}_{\Gamma\Omega} & \mathbf{M}_{\Gamma\Gamma} \end{bmatrix} \ddot{\mathbf{u}} + \begin{bmatrix} \mathbf{C}_{\Omega\Omega} & \mathbf{C}_{\Omega\Gamma} \\ \mathbf{C}_{\Gamma\Omega} & \mathbf{C}_{\Gamma\Gamma} \end{bmatrix} \dot{\mathbf{u}} + \begin{bmatrix} \mathbf{K}_{\Omega\Omega} & \mathbf{K}_{\Omega\Gamma} \\ \mathbf{K}_{\Gamma\Omega} & \mathbf{K}_{\Gamma\Gamma} \end{bmatrix} \mathbf{u} = \begin{bmatrix} \mathbf{p}_{\Omega\Omega} \\ \mathbf{p}_{\Gamma\Gamma} \end{bmatrix} - \begin{bmatrix} \mathbf{0} \\ \mathbf{p}_b \end{bmatrix}. \tag{3}$$

Nodes at the near-field are contained in blocks with subscript "$\Omega\Omega$" while nodes at the far-field are contained in blocks with subscript "$\Gamma\Gamma$". The coupling of near-field and far-field is contained in those blocks marked with the subscripts "$\Omega\Gamma$" and "$\Gamma\Omega$". The response of the infinite half space is represented by the vector $\mathbf{p}_b$ that acts only at the boundary Γ, so that the far-field influence can be applied to the near-field as a load. More information on how $\mathbf{p}_b$ is computed can be found in [8]. To compute the far-field's response the convolution integral needs to be solved. This is from computational point of view very costly. In order to reduce the very high computational effort, different model reduction techniques are used, as described in [9]. The damping is here taken into account by applying the Rayleigh representation

$$\mathbf{C} = c_m\mathbf{M} + c_k\mathbf{K}\,. \tag{4}$$

The parameters c_m and c_k are determined, by solving the structures eigenvalue problem, they can be derived from the first two natural frequencies [10].

2.2 CFD water waves simulations

The water waves simulation is carried out with the interFoam solver available in the OpenFoam C++ libraries [11]. This consists in a finite volume method to solve the viscous fluid flow equations, together with a volume-of-fluid strategy for the two-fluid flow case. The governing equations of a two-phase, incompressible, viscous and laminar flow can be expressed in the following manner

$$\frac{\partial\rho}{\partial t} + \nabla\cdot(\rho\mathbf{U}) = \mathbf{0}; \tag{5}$$

$$\frac{\partial\rho\mathbf{U}}{\partial t} + \nabla\cdot(\rho\mathbf{U}\mathbf{U}) - \nabla\cdot\left(\mu(\nabla\mathbf{U} + \nabla\mathbf{U}^T)\right) = -\rho\mathbf{g} - \nabla p; \tag{6}$$

$$\frac{\partial\alpha}{\partial t} + \nabla\cdot(\mathbf{U}\alpha) + \nabla\cdot(\mathbf{U}_C\,\alpha(1-\alpha)) = \mathbf{0}; \tag{7}$$

where $\mathbf{U}$ is the fluid velocity, p the pressure, ρ the fluid density, μ the dynamic viscosity, α the phase fraction and $\mathbf{U}_C$ the artificial compressive velocity. The phase fraction α describes the fluid distribution in the domain, being $0 \leq \alpha \leq 1$, with 0 for the denser fluid and 1 for the lighter one, being the interface position at $\alpha = 0.5$. Furthermore, $|\mathbf{U}_C| = \min(c_\alpha|\mathbf{U}|, \max(|\mathbf{U}|))$, where c_α is the artificial interface compression [12, 13]. The fluid properties like density and viscosity are determined in each phase as a function of the fluid fraction.

To generate the waves in the numerical wave tank, the static boundary wave generation technique described and developed by [14] is employed. This boundary condition is part of the OpenFoam libraries and it enables to generate several kinds of water waves according to the well known theories of Stokes I (linear waves), Stokes II (second order waves), Stokes V (high order waves), Boussinesq solitary waves, etc. These boundary conditions allow to control with accuracy the characteristics of the generated waves, such as the wave height, wave number, and wave period, among others. On the other hand, wave absorption techniques are used at the outlet and inlet boundaries to avoid nonphysical wave reflections. These active wave absorbing boundary conditions also enable to reduce the size of the computational domain and the cost of the simulations. In this work, the static boundary wave absorption techniques developed in [14] are used.

2.3 Non-matching meshes solution projection

Since the fluid flow domain discretization is much more refined than that of the wind turbine pile, particularly at the region where the free surface moves, a solution projection algorithm is used to transfer the pressure from the vertices of the fluid mesh to those of the structure mesh. Afterwards, the nodal forces are computed at the surface of the wind turbine pile by integration of the pressure. To carry out this task, a state projection library based on the Nearest Neighbor projected algorithm is used. This library has been described, validated and previously employed by the authors in [4] to transfer the forces and displacements in the numerical solution of soil-structure interaction problems using non-matching meshes. On the other hand, a one-directional coupling is considered in the current research as a first approach since it is assumed that the displacement of the solid boundary does not have an appreciable influence on the fluid behavior. Therefore, only the pressure is transferred from the fluid to the solid mesh. Also, the fluid flow problem and the wave loads can be solved beforehand, independently.

3 Offshore wind turbine under water waves and wind

To analyze the behavior of the offshore wind turbine different third-party software packages as well as different in-house computer codes are combined. The general work flow is shown in Fig. 1. Finite element meshes and scaled boundary finite element meshes are generated by using the geometry and mesh generation toolkit CUBIT [15]. Here the geometry is created as well as the final meshes. The eigenvalue problem is solved using GNU Octave [16] to compute the eigenvalues and eigenvectors of the wind turbine and its foundation. Aerodynamic loads are generated by using FAST [17] from National Renewable Energy Laboratory and wave loads are generated by using OpenFoam C++ libraries [11]. StateProjection is used to transfer the loads from the finer fluid mesh to the FEM mesh of the tower (further information in section 2.3). ParaView [18] is utilized for visualization of the results of the three dimensional model. Time displacement records of chosen nodes can optionally transferred into frequency domain by applying FFT for model assessment and evaluation.

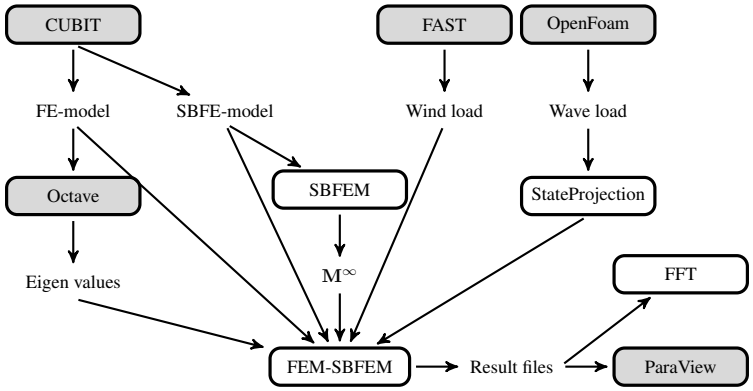

Figure 1. Flow diagram of virtual offshore wind turbine analysis. Boxes filled in gray are commercial or open source software packages.

3.1 Wind turbine and windloads

The design of the numerically investigated offshore wind turbine is given by a reference wind turbine, which has been analyzed by the National Renewable Energy Laboratory (NREL)[19]. The wind turbine is a 5 MW plant, with an upwind rotor of 126 m in diameter. The hub height is 90 m. Rotor and nacelle have a mass of 110000 kg and 240000 kg, respectively. Both are mounted on a 87.6 m-height steel tower, which has a diameter of 3.87 m on top and 6 m. at the bottom. The towers wall thickness changes linearly with increasing height from 0.0351 m to 0.0247 m. The tower has a mass of 347460 kg, so that entire wind turbine has a mass of 697460 kg, which is founded on a cylindrical foundation. For the numerical analysis the tower is modeled by three dimensional continuum elements. The mass of rotor and nacelle is taken into account by mass elements, which are distributed at the towers very top. The tower is made of steel using the following material parameters: Young's modulus $E = 2.1 \cdot 10^{11}$ N/m^2, Poisson's ratio $\nu = 0.3$ and density $\rho = 8500$ kg/m^3. The density of steel is increased by 7.65% to take the technical equipment within the tower into account [19]. Foundation and soil are modeled by three dimensional continuum elements. The finite element mesh is refined in the center and becomes more coarse to the outside. This is shown in Figs. 2(a) and 2(b). The cylindrical reinforced concrete foundation has the material parameters: Young's modulus $E = 4.896 \cdot 10^{10}$ N/m^2, Poison's ratio $\nu = 0.2$ and density $\rho = 3054$ kg/m^3. The surrounding soil is modeled as a homogeneous isotropic half-sphere with a radius of 102 m. It consists of close sand with the material parameters: Young's modulus $E = 1.5 \cdot 10^8$ N/m^2, Poison's ratio $\nu = 0.25$ and density $\rho = 2200$ kg/m^3. The wind turbine's tower is mounted to the foundation directly. Here no fixed-base boundary conditions are applied. The infinite half-space is discretized by scaled boundary finite elements. The nodes and elements are located at the common interface for the finite element model and the scaled boundary finite element model. The scaling center is located in the domains center directly beyond the towers bottom with the global coordinates $SC = \{0, 0, 0\}$.

For the computation of the turbulent aerodynamic loads, a reference speed of 12 m/s was used. The turbulent wind field model used corresponds to the spectral and exponential coherence model of Kaimal. The loads F_x and F_y act in fore-aft direction and side-side direction, respectively. F_z acts in axial direction. The moments M_x, M_y, and M_z are roll, pitch and yaw moments, respectively. The loads have to be distributed to the top nodes of the system and are shown in Fig. 2(c).

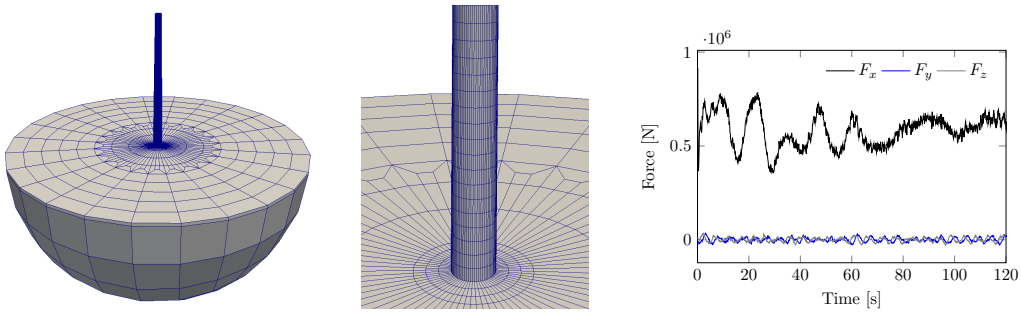

(a) Mesh of tower, foundation and soil.

(b) Mesh at the bottom of the tower.

(c) Windloads at the top of the tower.

Figure 2. Grid for the FEM-SBFEM problem and the Windloads.

3.2 Vertical cylinder under regular non-linear water waves

As a first step in the numerical analysis, the wave loads exerted on a vertical cylinder are computed. To this end, the experimental results obtained by [20] in the Danish Hydraulic Institute and the numerical results shown in [3] are taken as reference for validation.

A vertical cylinder of radius $a = 0.125$ m is placed inside a prismatic computational domain that, with convenient boundary conditions, represents half of the full problem extents, see Fig. 3(a). The numerical domain has width $W = 16a = 2$ m, length $L = 15$ m and height $H_c = 1.01$ m. The water depth is $h = 0.505$ m. The cylinder center is placed 7.5 m from the inlet, and only one half is represented. The boundary condition for the velocity at the lateral walls and cylinder surface is perfect slip. At the bottom of the channel a zero velocity boundary condition is set. A symmetry condition is applied at the vertical symmetry plane along the water channel. At the top of the domain, the `pressureInletOuletVelocity` condition of OpenFoam is used, which sets a zero gradient condition to the velocity of the outflow boundary and a velocity based on the flux in the patch-

normal direction of the inflow boundary. The fluid properties are: $\rho_l = 1000\ \mathrm{kg/m^3}$ and kinematic viscosity $\nu_l = 1.0 \cdot 10^{-6}\ \mathrm{m^2/s}$ for the water, and $\rho_a = 1\ \mathrm{kg/m^3}$ and $\nu_a = 1.48 \cdot 10^{-5}\ \mathrm{m^2/s}$ for the air.

At the inlet boundary, the wave generation is characterized by the second order Stokes II wave model [1]. The characteristic wave parameters are those defined in [3], namely wave height $H = 0.0726\ \mathrm{m}$ and wave period $T = 1.22\ \mathrm{s}$. Then, it follows that the wave length is $\lambda = 2.11\ \mathrm{m}$, wave number $k = 2.96$, and celerity $c = 1.73\ \mathrm{m/s}$. Both at the inlet and the outlet dynamic absorbing boundary conditions are set in order to avoid wave reflections. This absorbent boundary condition is based on the linear shallow water theory introduced by [21] and further extended in [14] to three dimentional problems.

The numerical model was solved with two discretizations. The results presented here correspond to the finer one, which is a multi-block grid of 1.3 million cells generated with the `blockMesh` utility. This is shown in Fig. 3(b), where it can be seen the two refinement levels in the region where the free surface is expected to move and also close to the cylinder surface. The characteristic lengths of the cells are: $\Delta x = \lambda/38$ along the length of the water channel, $\Delta y = \lambda/38$ along its width and $\Delta z = H/13$ along its height, at the refined region close to the free surface. The model was solved with the following parameteres for the interFoam solver: maximum Courant number $C_o = 0.1$ giving a variable time step, time scheme Backward-Euler, linear upwind for the finite volume velocity scheme and a MULES scheme for the α equation. The chosen interface compression, $c_\alpha = 0.75$, led to a free surface smeared within 3 to 4 cells width.

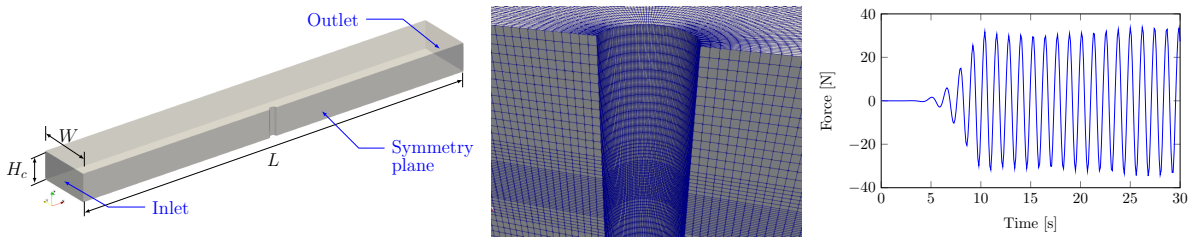

(a) Fluid domain for the wave problem.

(b) Fluid mesh at the region close to the cylinder.

(c) Horizontal load in time domain.

Figure 3. Domain, grid and forces for the fluid problem.

The loads exerted by the fluid over the vertical cylinder in the waves direction are shown in Fig. 3(c). The resultant horizontal force shows a quasi-periodical behavior in time, after the initial transient stage, with a maximum value $F_{x,\max} \simeq 34\ \mathrm{N}$. This result agrees well with the numerical value computed by [3] and also with the experimental result obtained in [20], which are both of them $F_{x,\max} \simeq 32.4\ \mathrm{N}$. Also the maximum horizontal force predicted with the Morison equation is $F_{x,\max} \simeq 32.6\ \mathrm{N}$.

Surface elevation in time measured at certain gauge points as well as frequency analysis with fast Fourier transform of the horizontal force and surface displacement, not shown here by lack of space, also compare well to those shown in reference [3].

3.3 Scaling of the water waves loads

To calculate a rough estimate of the loads exerted by the waves on the real scale OWT pile, the following procedure is carried out, resulting in force magnitude and time scaling. Taking into account that the OWT pile diameter is $D_{\mathrm{pile}} = 6\ \mathrm{m}$ and in order to have the same ratio D/h than in the small cylinder case, the water depth should now be $h \simeq 12\ \mathrm{m}$. In the cylinder case the relative water depth is $h/(g \cdot T^2) = 0.0346$, therefore the wave period in the real scale problem should be $T = 5.95\ \mathrm{s}$ and the wave frequency $f \simeq 0.17\ \mathrm{Hz}$. To keep the same water wave model (i.e. Stokes II) the relative wave height value $H/(g \cdot T^2) = 0.0049$ of the cylinder case should be preserved, therefore the wave height of the OWT case must be $H = 1.7\ \mathrm{m}$. Finally, taking into account that the wave depth in the small cylinder case is $kh = 1.39$, the wave number for the OWT is $k = 0.116$ and the wave length $\lambda = 54.24\ \mathrm{m}$.

With the previously defined wave parameters, it is possible to estimate the maximum force magnitude with the Morison equation, given the fact that $D_{\mathrm{pile}}/\lambda = 0.11 < 0.15$ (see ref. [1]). Since the angular wave frequency is $\sigma = \sqrt{gk\tanh(kh)} = 1.0018\ \mathrm{rad/s}$, the maximum velocity magnitude of the water particles can be calculated using the Stokes II wave equations [1], which is $\max(|\mathbf{U}|) = 1.11\ \mathrm{m/s}$. Afterwards, the Reynolds number based on the pile diameter can be computed, namely $\mathrm{Re} \simeq 6.6 \cdot 10^6$. Taking into account the experimental correlations presented in [22] it is possible to obtain approximated values of the drag C_{D} and inertia C_{M} coefficients for unsteady oscillatory flows around vertical cylinders corresponding to this Reynolds number, namely $C_{\mathrm{D}} \simeq 0.6$

and $C_{\mathrm{M}} \simeq 0.6$. Finally, the maximum horizontal drag and inertia force components are

$$F_{D,\max} = \frac{1}{2}\rho C_{\mathrm{D}} U_{\max}^2 D_{\mathrm{pile}} h = 26613 \text{ N} \tag{8}$$

$$F_{I,\max} = C_{\mathrm{M}} \frac{\rho\pi D^2}{4k} \frac{H\sigma^2}{2} = 901632 \text{ N} \tag{9}$$

Therefore, as a first approach, the maximum horizontal force is $F_{x,\max} \simeq 0.93$ MN. It is also clear that inertia force dominates over drag force. Afterwards, the surface mesh of the small cylinder is scaled in order to have the same diameter as the OWT pile. Then, the total pressure computed on the surface of the small cylinder is post-processed in order to meet the maximum force previously calculated. To this end, for each time step the total pressure is decomposed in its hydrostatic and dynamic components. For each given mesh node on the surface of the scaled cylinder, the hydrostatic component is scaled considering the height of the water column, given by the position of the free surface above the node. On the other hand, the dynamic pressure is scaled by a given factor such that added to the scaled hydrostatic pressure and integrated on the surface of the OWT pile generates the maximum value $F_{x,\max} \simeq 0.93$ MN.

It is acknowledged that a 3D turbulent flow simulation of the water waves around the real scale OWT pile would provide more accurate results. However, taking into account the computational cost of such simulation, it is considered that the approach presented in this work is accurate enough to provide data to the FEM-SBFEM OWT model in order to test the coupling strategy and to carry out a dynamic analysis of the OWT structure. Currently, 3D simulations solving the RANS Navier-Stokes equations are under way both with OpenFoam and Reef3D [2].

3.4 Results

The simulation is conduct with a time step length $\Delta t = 0.01$ s for a total period of $T = 120$ s. Fig. 4(a) shows the results of the towers top displacement in x-, y- and z-direction under wave load. The wave load leads to a displacement of the tower head. Fig. 4(b) and 4(c) compare the loading situations wind, waves and wind+waves. The black line shows the displacement of the tower under wind and wave loads. Compared to the gray line, which describes the displacement under wind loads, the influence on the displacement at the top of the tower is small, but still the effect on the system becomes visible. When considering the base of the tower, the influence of the wave loading is greater. As a result of wave loading, oscillations of the displacement in x-direction from positive to negative values occur.

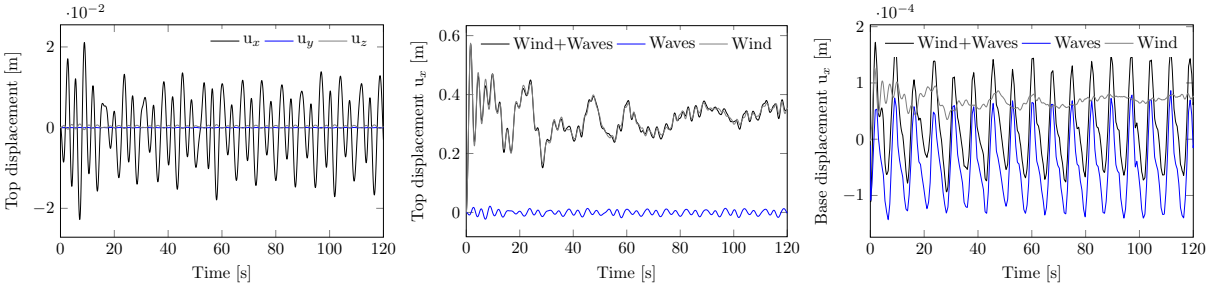

(a) Top displacement under wave load.

(b) Top displacement under aerodynamic and wave load.

(c) Base displacement under aerodynamic and wave load.

Figure 4. Top and base displacement of the offshore wind turbine.

4 Conclusions and outlook

In this article we presented a strategy to simulate an offshore wind turbine where wind and wave loads were considered. The wave loads were included from a computational fluid dynamics study with OpenFoam for second order Stokes waves. The action of the waves on a vertical cylinder in a water channel where analyzed and validated, finding a good agreement with respect to numerical, experimental and theoretical results from other authors. The fluid pressure on the pile of the wind turbine is obtained by scaling the size of the cylinder, as well as the wave characteristic parameters in order to keep the same kind of wave (i.e., second order Stokes) and afterwards using a non-matching solution projection algorithm. The proposed method is able to represent the effects of wave loads on the structure, taking into account wind and soil-structure interaction. The SSI is considered with the aid of a

coupled FEM-SBFEM approach in time domain. The offshore wind turbine is located in calm water, like the Baltic sea. In future works focused wave groups and breaking waves should be taken into account. This could be used to simulate offshore wind turbines subjected to larger forces due to wave loads.

Acknowledgements. The authors appreciate the support provided by the following projects: CAI+D 2020-50620190100140LI, CAI+D 2020-50620190100110LI, PICT-2018-01607, PICT-2018-02920, PID-UTN-8132.

Authorship statement. The authors hereby confirm that they are the sole liable persons responsible for the authorship of this work, and that all material that has been herein included as part of the present paper is either the property (and authorship) of the authors, or has the permission of the owners to be included here.

References

[1] R. G. Dean and R. A. Dalrymple. Water Wave Mechanics for Engineers and Scientists, volume 2 of Advanced Series in Ocean Engineering. World Scientific Publishing Co. Pte. Ltd., 1991.
[2] A. Aggarwal, P. D. Tomaselli, E. D. Christensen, and H. Bihs. Computational Fluid Dynamics Investigations of Breaking Focused Wave-Induced Loads on a Monopile and the Effect of Breaker Location. Journal of Offshore Mechanics and Arctic Engineering, vol. 142, n. 2, 2019.
[3] L. Chen. Modelling of Marine Renewable Energy. PhD Thesis, University of Bath - Department of Architecture and Civil Engineering, 2015.
[4] M. Schauer and G. R. Rodriguez. A coupled FEM-SBFEM approach for soil-structure-interaction analysis using non-matching meshes at the near-field far-field interface. Soil Dynamics and Earthquake Engineering, vol. 121, pp. 466–479, 2019.
[5] S. Bhattacharya, G. Nikitas, L. Arany, and N. Nikitas. Soil-Structure Interactions for Offshore Wind Turbines. Engineering and Technology Reference, vol. 2, 2017.
[6] M. Schauer, J. E. Roman, E. S. Quintana-Ortí, and S. Langer. Parallel computation of 3-D soil-structure interaction in time domain with a coupled FEM/SBFEM approach. Journal of Scientific Computing, vol. 52, pp. 446–467, 2012.
[7] N. Newmark. A method of computation for structural dynamics. Journal of Engineering Mechanics Division, vol. 85, pp. 67–94, 1959.
[8] J. Wolf and C. Song. Finite-Element Modelling of Unbounded Media. John Wiley & Sons, Chichester, 1996.
[9] M. Schauer. On the influence of far-field model reduction techniques using a coupled FEM-SBFEM approach in time domain. Journal of Mathematical Sciences and Modelling, vol. 1, 2018.
[10] M. Schauer, F. Taddei, and G. R. Rodriguez. Soil-structure interaction simulations taking into accout the transient propagation of seismic waves. In COUPLED VIII : proceedings of the VIII International Conference on Computational Methods for Coupled Problems in Science and Engineering, 2019.
[11] The OpenFOAM Foundation. https://openfoam.org/, 2021.
[12] S. S. Deshpande, L. Anumolu, and M. F. Trujillo. Evaluating the performance of the two-phase flow solver interFoam. Computational Science and Discovery, vol. 5, n. 1, pp. 36. Number: 1, 2012.
[13] B. E. Larsen, D. R. Fuhrman, and J. Roenby. Performance of interfoam on the simulation of progressive waves. Coastal Engineering Journal, vol. 61, n. 3, pp. 380–400, 2019.
[14] P. Higuera. Aplicación de la Dinámica de Fluidos Computacional a la Acción del Oleaje Sobre Estructuras. PhD thesis, Universidad de Cantabria - Dpto de Cs. y Técnicas del Agua y del Medio Ambiente, 2015.
[15] Sandia National Laboratories: New Mexico. CUBIT 13.2. https://cubit.sandia.gov/index.html.
[16] GNU Octave Scientific Programming Language. GNU Octave. https://www.gnu.org/software/octave/.
[17] NREL National Renewable Energy Laboratory. FAST v7. https://nwtc.nrel.gov/FAST.
[18] Kitware. ParaView 5.0.1. https://www.paraview.org/.
[19] J. Jonkman et al. Definition of a 5-MW reference wind turbine for offshore system development. Technical Report NREL/TP-500-38060, 2009.
[20] J. Zang, P. Taylor, G. Morgan, M. Tello, and J. Orszaghova. Experimental study of non-linear wave impact on offshore wind turbine foundations. In 3rd International Conference on the Application of Physical Modelling to Port and Coastal Protection (Coastlab2010), 2010.
[21] H. A. Schäffer and G. Klopman. Review of Multidirectional Active Wave Absorption Methods. Journal of Waterway, Port, Coastal, and Ocean Engineering, vol. 126, n. 2, pp. 88–97, 2000.
[22] R. Dean and P. Aagaard. Wave Forces: Data Analysis and Engineering Calculation Method. Journal of Petroleum Technology, vol. 22, n. 03, pp. 368–375, 1970.